

## Laponite intercalated biomimetic multilayer coating prevents glucocorticoids induced orthopedic implant failure

Zhe Liu<sup>a,1</sup>, Qian Tang<sup>a,1</sup>, Ruo-Tao Liu<sup>a,1</sup>, Ming-Zhao Yu<sup>a</sup>, Hao Peng<sup>a</sup>, Chang-Qing Zhang<sup>a,\*\*</sup>, Zhen-Zhong Zhu<sup>a,\*\*\*</sup>, Xiao-Juan Wei<sup>b,\*</sup>

<sup>a</sup> Department of Orthopedic Surgery, Shanghai Sixth People's Hospital Affiliated to Shanghai Jiao Tong University School of Medicine, 600 Yishan Road, Shanghai, 200233, China

<sup>b</sup> Institute of Microsurgery on Extremities, Shanghai Sixth People's Hospital Affiliated to Shanghai Jiao Tong University School of Medicine, 600 Yishan Road, Shanghai, 200233, China

### ARTICLE INFO

#### Keywords:

Layer-by-layer self-assembly  
Organic-inorganic hybrid  
Glucocorticoid  
Osseointegration  
Antibacterial

### ABSTRACT

Implant failure, which is commonly associated with failure of osseointegration and peri-implant infection, is a severe complication of orthopedic surgery. In particular, the survival rate of implants is significantly decreased in patients using long-term glucocorticoids (GCs). However, the exact molecular mechanism underlying GCs-induced implant loosening, as well as preventive strategies for these patients, is unclear. To address this problem, we performed RNA-sequencing and found that WNT16 was correlated with GCs-induced osteopenia (LogFC = -5.17,  $p < 0.01$ ). Inspired by the concept of “organic-inorganic” hybrid, we theorized to introduce a bioactive two-dimensional nanosheet into a layer-by-layer (LbL) self-assembly coating to construct a customized implant that targets WNT16. After screening commercially available nanosheets, laponite (LAP) was identified as a cost-effective rescuer for GCs-induced WNT16 inhibition, which was then intercalated into LbL deposition system consisting of quaternized chitosan (QCS) and hyaluronic acid (HA). The hybrid coating (QCS/HA/LAP) showed micrometer thickness and improved hydrophilicity and interface roughness. Furthermore, QCS/HA/LAP coated polyetheretherketone (PEEK) implant enhanced cell viability, adhesion, and osteogenic differentiation of bone marrow mesenchymal stem cells (BMSCs), and promoted osteointegration of PEEK in GCs-treated rats by targeting the WNT16/ $\beta$ -catenin axis. The assembled QCS has proven antibacterial properties, and the hybrid coating exerted potent detrimental effects against methicillin-resistant *Staphylococcus aureus* (MRSA) and *Escherichia coli* (*E. coli*), both *in vitro* and *in vivo*. Taken together, these results suggest that QCS/HA/LAP coating has great potential for use in implants customization, and has synergistic pro-osteogenic and antibacterial effects that help prevent implant failure in GCs-treated patients.

### 1. Introduction

Despite significant advances in orthopedic implants in recent decades, implant failure remains a major challenge [1,2]. The loosening rate over a 4–10-year follow-up after cementless total knee arthroplasty was as high as 28%, and the infection rate was 2–5% after joint prosthesis and internal fixation [3]. The situation is even worse in patients with osteoporosis, diabetes, or drug complications [4–6].

Glucocorticoids (GCs) are immunosuppressive agents commonly used for autoimmune and inflammatory diseases, such as asthma, systemic lupus erythematosus (SLE), and rheumatoid arthritis (RA) [7]. Patients receiving long-term GCs therapy experience rapid bone loss and an increased risk of infection, which results in an almost 1.5–2.5-fold increased request of revision surgery in these patients after primary surgical treatment [8–10]. However, few previous studies have drawn up the strategies to prevent implant failure in GCs-treated patients;

Peer review under responsibility of KeAi Communications Co., Ltd.

\* Corresponding author.

\*\* Corresponding author.

\*\*\* Corresponding author.

E-mail addresses: [zhangcq@sjtu.edu.cn](mailto:zhangcq@sjtu.edu.cn) (C.-Q. Zhang), [zzz1129@gmail.com](mailto:zzz1129@gmail.com) (Z.-Z. Zhu), [xjweish@163.com](mailto:xjweish@163.com) (X.-J. Wei).

<sup>1</sup> Zhe Liu, Qian Tang and Ruo-Tao Liu contributed equally to this work.

<https://doi.org/10.1016/j.bioactmat.2022.09.013>

Received 11 June 2022; Received in revised form 18 August 2022; Accepted 12 September 2022

2452-199X/© 2022 The Authors. Publishing services by Elsevier B.V. on behalf of KeAi Communications Co. Ltd. This is an open access article under the CC BY-NC-ND license (<http://creativecommons.org/licenses/by-nc-nd/4.0/>).

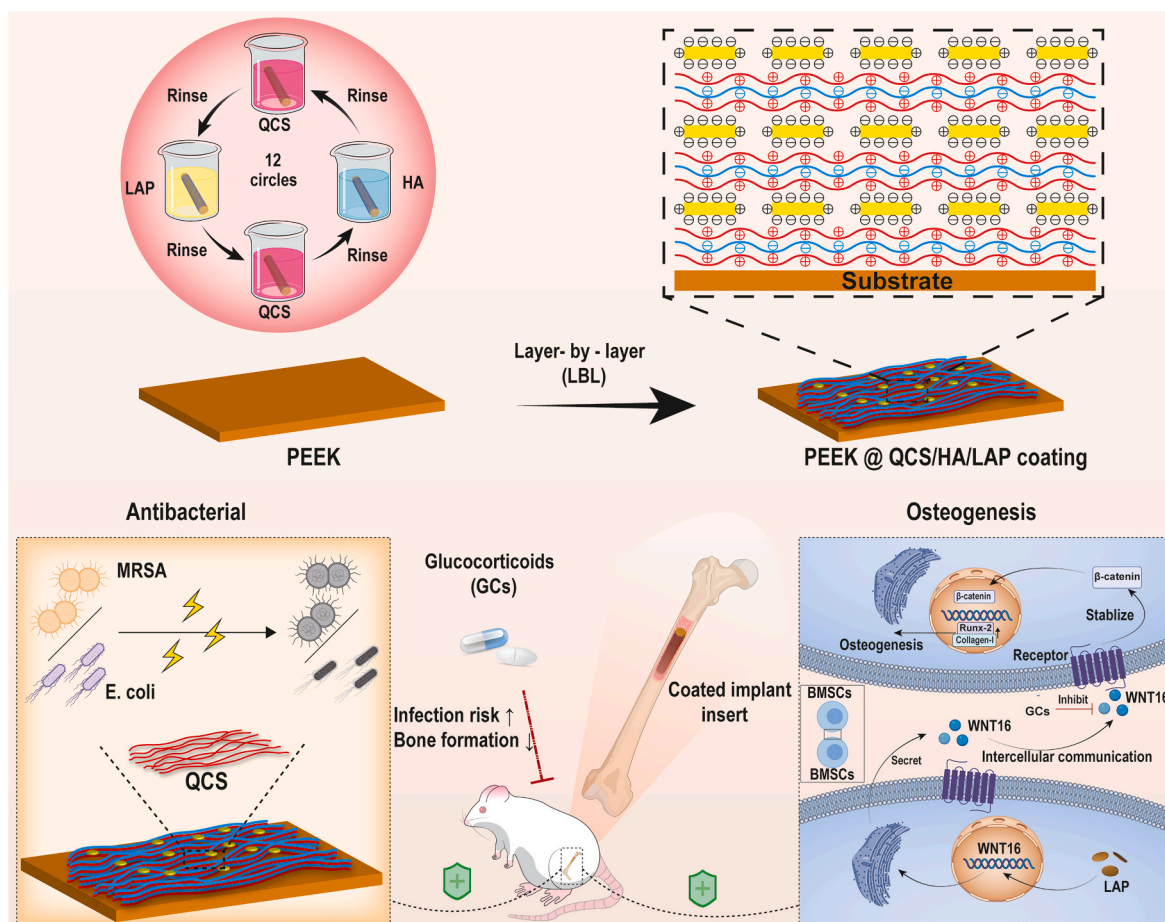
therefore, novel therapeutic approaches are needed to prevent implant failure in these patients.

Layer-by-layer (LbL) self-assembly is a facile and versatile technology for alternative deposition of polymers with complementary interactions under aqueous conditions [11,12]. It is used to fabricate functionally multilayered nanocomposites for biomedical applications, particularly implant coating [13–16]. LbL coating preserves the intrinsic mechanics of implants and converts the relatively inert interface to a bio-friendly interface, which attracts bone marrow mesenchymal stem cells (BMSCs) adhesion and therefore promotes osseointegration between the implant and surrounding tissues [13,17]. Moreover, with the development of “organic-inorganic” hybrid theory, several multilayered films assembled using traditional polymers with intercalated nanosheets or nanoparticles have been developed, which increase mechanical strength and have additional bioactivities [18,19]. Kotov et al. [19,20] reported a montmorillonite (MMT) intercalated LbL film that exhibited a “brick and mortar” structure, with maximal tensile strength and Young’s modulus of  $150 \pm 40$  MPa and  $13 \pm 2$  GPa, respectively. What’s more, inorganic nanomaterials, including nanoclays, graphite oxide (GO), MXene, MoS<sub>2</sub>, and other nanoparticles, were all reported to have promotive effects on osteogenesis [21,22]. Thus, such a hybrid structure is suitable for orthopedic implant coating due to its mechanical and biological properties. On the other hand, for the basic building blocks selection, polysaccharides (e.g., chitosan [CS] and hyaluronic acid [HA]) are the first choice, since they are potent antimicrobial agent (CS) and natural constituents of extracellular matrix (HA) respectively, along with favorable biocompatibility and biodegradability [23]. Of note, traditional CS dissolves only in acidic conditions, and its antibacterial effect is inhibited at pH > 6.5 [24]. This problem can be solved by chemical

modification. 2-hydroxypropyltrimethyl ammonium chloride chitosan, also called quaternized chitosan (QCS), is a derivate of CS, which is soluble in physiological pH and has higher antimicrobial activity [24]. Although no previous study has constructed inorganic nanomaterials intercalated QCS/HA film for implant coating, its potential pro-osteogenic and antibacterial properties are of significant interest and properly cater to the demands for preventing GCs induced implant failure.

The mechanism underlying inhibition of implant osseointegration by GCs remains elusive. It is well-known that excessive GCs induce apoptosis of osteoblasts (OBs) and osteocytes (OCs), and inhibit the osteogenesis of OBs. Wnt/ $\beta$ -catenin, Notch, autophagy-related signaling molecules, etc. were proven to be associated with this process [7]. In contrast, instead of OBs and OCs, the osseointegration of implant are more likely to be associated with BMSCs, and the surrounding micro-environments, which focus on recruiting intrasosseous BMSCs to construct a bridge across bone-to-implant interface [25,26]. Inhibition of Wnt signaling impedes osteogenesis of BMSCs on the bone-to-implant interface in older, postmenopausal, and hyperlipidemic patients, but has not yet been studied in GCs users [27–29]. Hence, the relationships as well as the underlying mechanisms between GCs intervention, BMSCs, and the peri-implant interface, are needed to be determined to develop targeted and customized therapeutic strategies.

In the present study, RNA-sequencing was used to identify potential molecular mediators of BMSCs in GCs-treated individuals, which identified WNT16 as a novel target. Subsequently, laponite (LAP), an artificial nanoclay with high stability and dispersibility [30,31], was demonstrated to promote WNT16 expression during the screening of several commercially available nanosheets. Based on these findings, we



**Scheme 1.** Schematic diagram of the preparation of multifunctional QCS/HA/LAP coating on PEEK substrates, and its application for preventing GCs-induced implant failure.

fabricated a LAP intercalated multilayered coating (QCS/HA/LAP) on an emerging polyetheretherketone (PEEK) implant, and systemically evaluated its pro-osteogenic and bactericidal effects *in vitro* and *in vivo* (Scheme 1). To best of our knowledge, this is the first study to construct a multifunctional organic-inorganic hybrid LbL coating for targeted prevention of GCs-induced implant failure.

## 2. Materials and methods

The detailed experimental methods can be found in the Supplemental Information file.

## 3. Results

### 3.1. Potential molecular mechanism underlying GCs-induced osteopenia

High-throughput RNA sequencing was performed to identify potential molecular targets in GCs-treated osteopenia. Successful establishment of the animal model was confirmed by micro-CT, which showed significant trabecular bone loss in GCs-treated rats; while the thickness and BMD of cortical bone was not altered significant by GCs treatment (Fig. S1). Furthermore, as shown in the MA plot (Fig. 1A), differentially expressed genes (DEGs), including 226 upregulated and 238 down-regulated genes, were identified ( $|\log_{2}FC| > 1$ ,  $p < 0.05$ ). To classify the functions of these DEGs, GO enrichment analysis was performed, which showed that upregulated DEGs were involved in the negative regulation of immune cells or inflammatory response, whereas most down-regulated DEGs were associated with cell morphology, OB differentiation, and bone mineralization (Fig. 1B). It suggested that GCs had negative effects on autoimmunity and osteogenesis. Moreover, a heatmap was constructed to visualize the top-10 upregulated and top-10 downregulated DEGs according to Pearson's correlation (Fig. 1C). WNT16, a member of the canonical Wnt signaling pathway, was one of the top-3 downregulated DEGs in GCs-treated rats ( $\log_{2}FC = -5.17$ ,  $p < 0.01$ ). To verify the RNA-sequencing data, protein levels of BMSCs derived from Ctrl and GCs-treated rats were evaluated. First, flow cytometry was applied to identify the surface markers of isolated BMSCs (Fig. S2). Both two BMSC types showed high expression of CD29, CD44, and CD90 (mesenchymal stem cell markers), but negative for CD34 and CD45 (hematopoietic cell markers). According to the Western blot results, the expression of WNT16/ $\beta$ -catenin axis is relatively downregulated in GCs-BMSCs (Fig. 1D–E). Similarly, in comparison with Ctrl-BMSCs, the ALP secretion and mineralization of GCs-BMSCs after osteogenic induction, were significantly decreased (Fig. 1F and G). Histologically, in addition, the femoral section of GCs-treated rats showed significantly lower trabecular bone mass, as well as down-regulated expression of collagen I and WNT16 *in vivo* (Fig. 1H and I).

### 3.2. Effect of LAP on osteogenic differentiation of GCs-treated BMSCs and its underlying mechanism

The effects of seven commercial nanosheets (MMT, layered double hydroxide (LDH), LAP, GO, MoS<sub>2</sub>, MXene, and BP) on WNT16 expression were evaluated. Western blot analysis of proteins derived from GCs treated BMSCs showed that MMT ( $p < 0.05$ ), LAP ( $p < 0.01$ ), GO ( $p < 0.05$ ), MXene ( $p < 0.05$ ), and black phosphorus (BP) ( $p < 0.05$ ) significantly increased the WNT16 level (Fig. 2A–B). Based on its good dispersibility and low cost [32–34], LAP was selected for subsequent experiments. As shown in Fig. S3A, no significant cell toxicity was observed on 0–100  $\mu\text{g}/\text{mL}$  of LAP treatment groups in 1-, 3-, and 7-days, but the 150  $\mu\text{g}/\text{mL}$  of LAP treatment group decreased the cell viability in 7-days, which supported that the good biocompatibility of LAP under 100  $\mu\text{g}/\text{mL}$  on BMSCs. Meanwhile, LAP treatment reversed the GCs-induced inhibition of cell viability in a dose-dependent manner (0–50  $\mu\text{g}/\text{mL}$ ) in 3-days, but no significant differences were observed between 50  $\mu\text{g}/\text{mL}$  and 100  $\mu\text{g}/\text{mL}$  of LAP treatment groups (Fig. S3B).

Furthermore, GCs administration significantly inhibited WNT16/ $\beta$ -catenin activity, as well as the expression of related osteogenic markers (collagen-I, RUNX2, and OCN). In addition, LAP treatment (0–50  $\mu\text{g}/\text{mL}$ ) attenuated these effects in a dose-dependent manner; however, for 50 and 100  $\mu\text{g}/\text{mL}$  of LAP treatment groups, although there was a slight increased tendency, but the significant differences were only shown in OCN, WNT16 and  $\beta$ -catenin (N) expression (Fig. 2C–F). Accordingly, LAP treatment of cells attenuated GCs-induced inhibition of ALP secretion and mineralization (Fig. 2G and H). Furthermore, immunofluorescence (IF) staining of collagen-I, OCN, WNT16, and  $\beta$ -catenin revealed significantly increased signals in LAP-treated groups, with higher staining intensity seen with higher concentrations (Figs. 2I and S4), the tendency was in accordance with the results of Western blot. Importantly,  $\beta$ -catenin expression varied in accordance with changes in WNT16 expression.

### 3.3. Fabrication and characterization of QCS/HA/LAP coating

Quartz crystal microbalance with dissipation (QCM-D) was used to monitor the LbL process for the first four circles of QCS/HA/LAP films on the gold substrates. The frequency shifts ( $\Delta F$ ) and dissipation differences ( $\Delta D$ ) produced at harmonic  $n = 3$  were plotted against the number of layers deposited (Fig. 3A). Overall, frequency shifts decreased, while dissipation gradually increased, with increasing deposition. Notably, there was a decrease in dissipation and slight increase in frequency shift upon assembly of the QCS and LAP layer, suggesting that film densification and water extrusion may occur when the molecules are deposited on HA-covered films. The *in vitro* and *in vivo* degradative tests showed that the area of residual coating stained with alcian blue was larger in EDC-treated samples than samples without EDC treatment. The delayed degradation of coating was related to the covalent binding of QCS and HA. Moreover, even though the original staining intensity of QCS/HA coating (which contained more HA) was stronger than that of QCS/HA/LAP coating, the latter is displayed slightly slower degradation rate than the former, suggesting that the hybrid structure was more stable (Figs. 3B and S5). Considering the relatively long period required for implant osteointegration, we applied crosslinked coating on the implant surface for subsequent experiments. Scanning electron microscopy (SEM) was used to characterize the surface morphology of substrates. As shown in Fig. 3C, compared to the relatively smooth surface in the PEEK and PEEK@QCS/HA group, the surface of QCS/HA/LAP coated PEEK was somewhat rough. The cross-sectional view showed that both coatings had a tight structure, but the coating was thicker and rougher in the QCS/HA/LAP than QCS/HA group. This may be because pure polymer coating was more homogeneous than the organic-inorganic hybrid structure. Meanwhile, energy-dispersive X-ray spectrometry (EDS) mapping showed that the coating was primarily a composite of C, O, Mg, and Si elements (Fig. 3D). Although lithium could not be detected by EDS, the presence of Mg and Si confirmed successful intercalation of LAP into the multilayers. Na, P, and Cl were detected because QCS and HA were dissolved in PBS. Atomic force microscopy (AFM) showed similar results to SEM (Fig. 3E), indicating that both coating surfaces had a nanoscale topography; the surface was rougher for the PEEK@QCS/HA/LAP group ( $R_q = 52.94 \pm 6.61$ ) than PEEK@QCS/HA group ( $R_q = 15.44 \pm 3.19$ ). Additionally, as shown in Fig. 3F, the contact angles of the QCS/HA ( $42.65 \pm 3.29^\circ$ ) and QCS/HA/LAP ( $28.98 \pm 2.82^\circ$ ) surfaces were smaller than the bare PEEK surface angle ( $68.40 \pm 4.08^\circ$ ), indicating that the LbL coating, particularly the LAP intercalated films, significantly improved implant surface wettability. The adhesion strength between coatings and PEEK substrates were evaluated by the Micro-scratch test. The L values corresponding with the failure location of coatings. As is shown in Fig. S6, the scratch length of QCS/HA scratches to the substrate was 0.6249 mm with the load at 2125 mN. The scratch length of QCS/HA/LAP scratches to the substrate was 1.3314 mm, and the load was 3362 mN. There were no significant cracks around the scratches, indicating good adhesion between the coatings and the

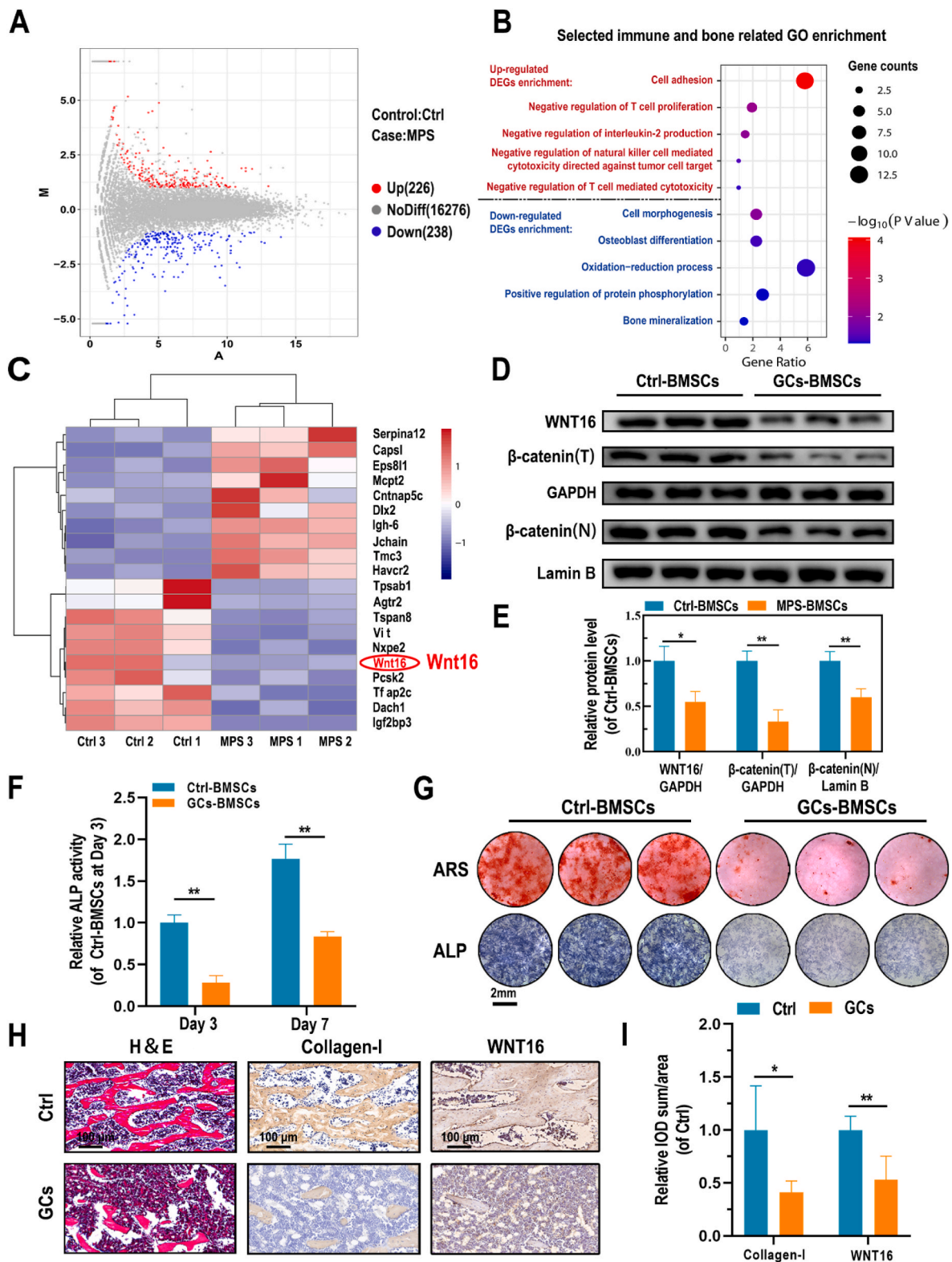


**Fig. 1.** Underlying molecular mechanism for GCs-BMSCs. (A) MA plot of DEGs of BMSCs derived from GCs-treated and Ctrl SD rats (red represents upregulated DEGs and blue represents downregulated DEGs). (B) Immune- and bone-related GO enrichment based on DEGs (C) Heatmap of the top-10 upregulated and downregulated DEGs. (D, E) Protein levels of WNT16 and  $\beta$ -catenin (total and nuclear protein levels) in Ctrl- and GCs-BMSCs. (F) Quantification of ALP activity of Ctrl- and GCs-BMSCs after 3 and 7 days of culture in osteogenic induction medium. (G) ALP and ARS staining of cells, as indicated, after 7 and 14 days of culture in osteogenic induction medium, respectively. (H, I) H&E and IHC staining (collagen-I and WNT16) results of femurs in Ctrl- and GCs-BMSCs treated rats. Data are mean  $\pm$  SD. Significant differences among groups are indicated (\*\* $p < 0.01$ , \* $p < 0.05$ ).

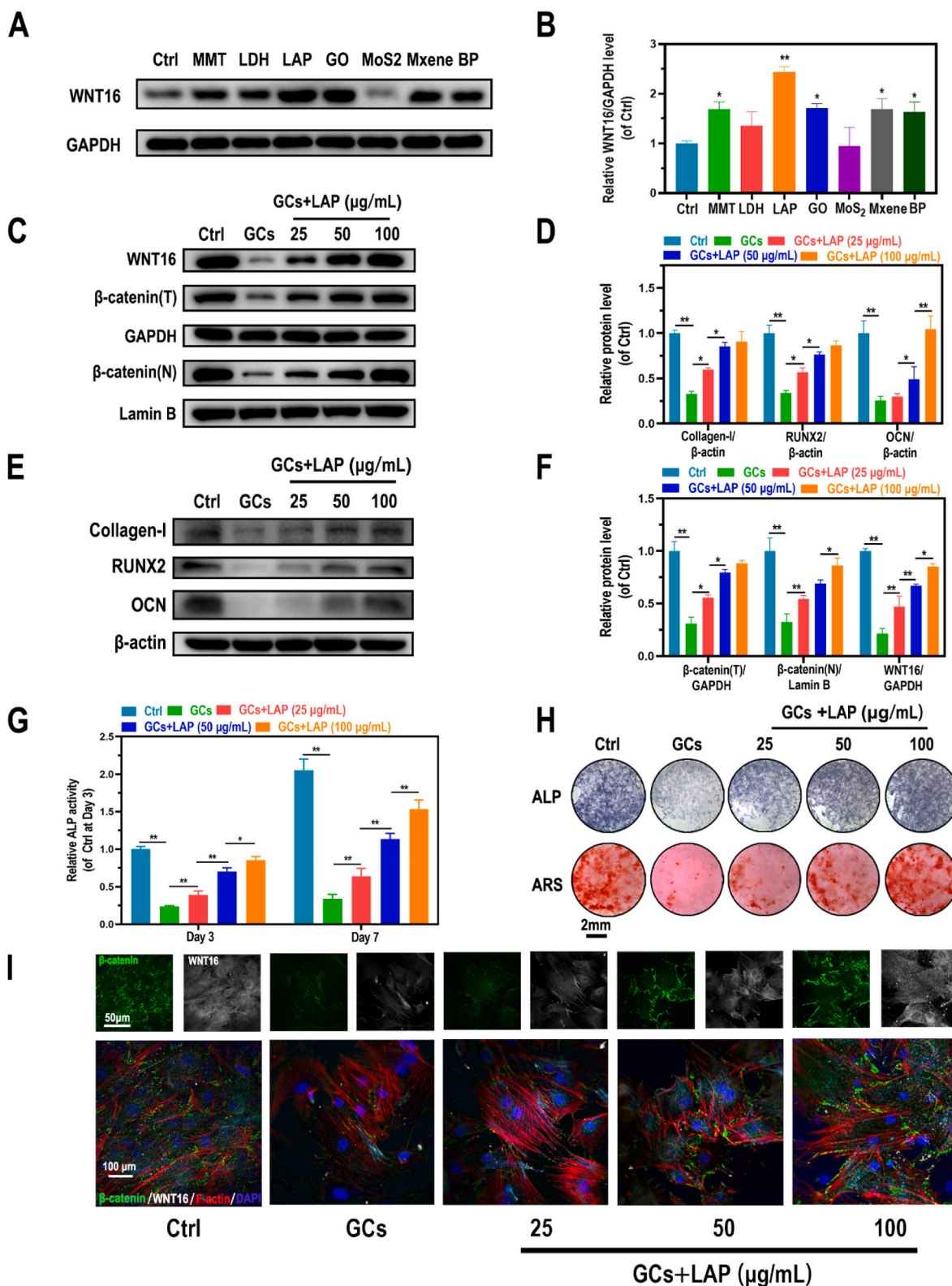


**Fig. 2.** Effects of LAP on GCs-treated BMSCs exerted via WNT16 activation. (A, B) Protein level of WNT16 in GCs pretreated BMSCs administrated with commercial nanosheets. (C-F) Protein levels of collagen-1, Runx-2, OCN, WNT16, and β-catenin (total and nuclear protein levels) in GCs-induced BMSCs treated with ascending LAP concentrations. (G) Quantification of ALP activity of Dex-induced BMSCs treated with ascending LAP concentrations. (H) ARS and ALP staining of Dex-induced BMSCs treated with ascending LAP concentrations. (I) IF staining of WNT16 (grey), β-catenin (green), F-actin (red), and DAPI (blue) in GCs-induced BMSCs treated with ascending LAP concentrations. Data are mean ± SD. Significant differences among groups are indicated (\*\*p < 0.01, \*p < 0.05).

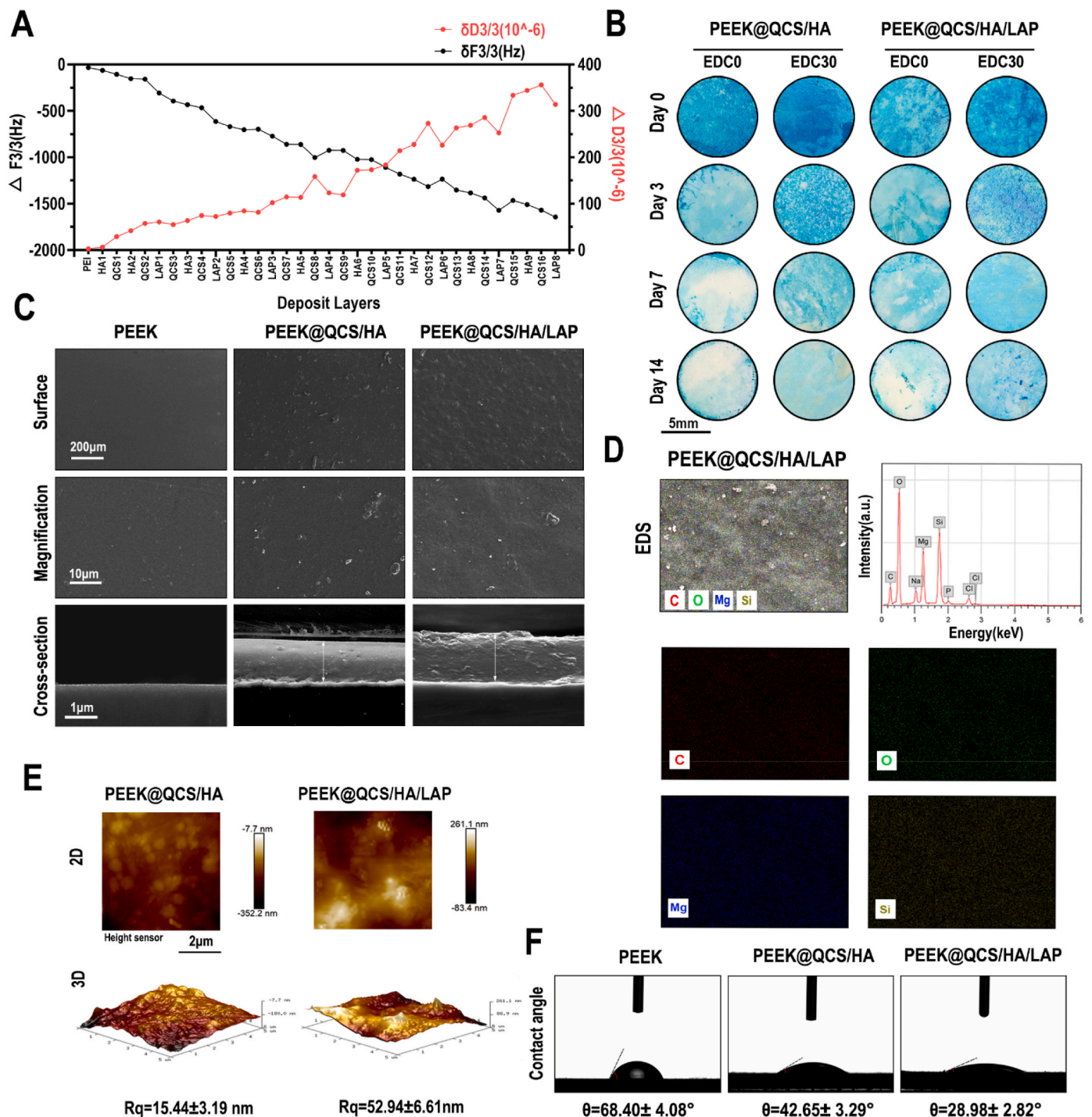


**Fig. 3.** Characteristics of QCS/HA/LAP coating. (A) QCM-D data of QCS/HA/LAP film build-up, frequency shifts, and dissipation of overtones ( $n = 3$ ). (B) Degradation test for QCS/HA and QCS/HA/LAP coatings with or without EDC crosslinking. (C) SEM image of the surface and cross-sectional morphology of bare and coated PEEK films. (D) EDS mapping showing the element distribution in QCS/HA/LAP coatings. (E) AFM images of the surface morphology and roughness of coatings. (F) Contact angles of bare and coated PEEK films.

substrate. It also implied that the adhesive strength of the coating prepared by “inorganic-organic” hybrid method was stronger than the solely polymer assembly. It could be due to the potential chelation bonds formed between LAP and polysaccharides, and the barrier effects of LAP layer have been incorporated into the LbL multilayer coating.

Furthermore, the loading amounts of LAP and release kinetics of LAP from QCS/HA/LAP coating were indirectly reflected by detecting the amounts of Li, Mg, and Si elements before and after LbL process, and the releasing behavior of these elements, respectively. The results showed

that there are about ~20–25% of LAP loaded (Li,  $22.41 \pm 4.30\%$ ; Mg,  $21.54 \pm 5.46\%$ ; Si,  $24.11 \pm 5.98\%$ ), after LbL process (Fig. S7A). According to the releasing profile, all of three elements could cumulatively release for over 35 days, but the most amounts were released in the first week (Figs. S7B–D).

### 3.4. In vitro biocompatibility and osteogenic activity of coated substrates

To determine the biocompatibility and bioactive effects of different

coated PEEK substrates on cells, GCs pretreated BMSCs were directly seeded on the surface of bare PEEK, QCS/HA-coated PEEK, and QCS/HA/LAP-coated PEEK. The CCK-8 analysis showed that a greater number of cells were implanted onto the coated surface, particularly in the PEEK@QCS/HA/LAP group (Fig. S8). In addition, as shown in Fig. S9, the hemolysis ratios of the PEEK, PEEK@QCS/HA, and PEEK@QCS/HA/LAP groups were  $1.05 \pm 0.35\%$ ,  $0.92 \pm 0.24\%$ , and  $1.42 \pm 0.33\%$ ,

respectively, implying that these implants had high hemocompatibility. Furthermore, TRITC-phalloidin staining of cells cultured for 1, 3, and 7 days showed that the cells in bare PEEK substrates had a round shape and loss of actin staining, while those in multilayer-coated substrates showed significant improvement, with a flat and diffuse morphology (Fig. 4A). Similar results were revealed by SEM images (Fig. 4B). Moreover, according to the Transwell assay, the migration ability of

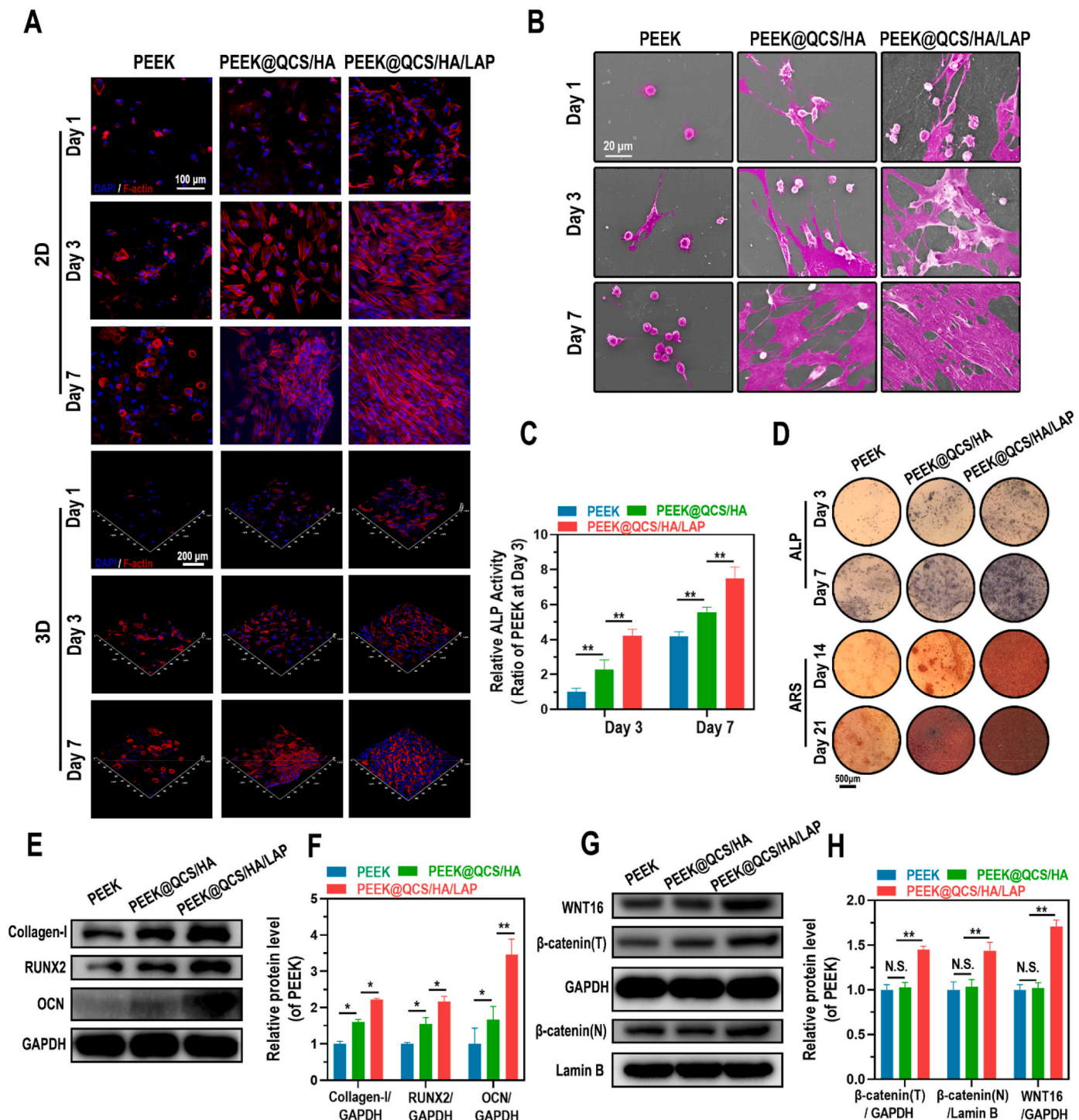


Fig. 4. Morphology and osteogenic differentiation of GCs-BMSCs seeded on QCS/HA/QCS/LAP coating. (A) CLSM images of F-actin staining of cells implanted on different surfaces on days 1, 3, and 7. (B) SEM images of cells implanted on different surfaces, as indicated, on days 3 and 7. (C) Quantification of ALP activity of BMSCs on different surfaces, as indicated, on days 3 and 7. (D) ALP and ARS staining of BMSCs seeded on different surfaces on days 3 and 7, and 14 and 21, respectively. (E-H) Protein levels of collagen-1, Runx-2, OCN, WNT16, and  $\beta$ -catenin (total and nuclear protein levels) in BMSCs on different surfaces. Data are mean  $\pm$  SD. Significant differences among groups are indicated (\*\* $p < 0.01$ , \* $p < 0.05$ ).

BMSCs was significantly higher in the PEEK@QCS/HA than PEEK group, while there was greater migration of BMSCs in the PEEK@QCS/HA/LAP than PEEK@QCS/HA group (Fig. S10). The osteogenic differentiation ability of cells differed among surfaces, with ALP secretion and mineralization levels being highest for PEEK@QCS/HA/LAP, followed by PEEK@QCS/HA and then bare PEEK (Fig. 4C and D). Accordingly, the protein levels of collagen-I, Runx2, and OCN were significantly increased in the PEEK@QCS/HA/LAP group compared to the PEEK and PEEK@QCS/HA groups. Moreover, QCS/HA coating also promoted the expression of these osteogenic markers, but the increased expression was not as evident as with the QCS/HA/LAP coating (Fig. 4E–F). Notably, WNT16/ $\beta$ -catenin axis activation was only shown in LAP intercalated coating group (Fig. 4G–H).

### 3.5. *In vivo* osseointegration evaluation

As shown in Fig. S11, except for mild hepatic steatosis in GCs-treated rats, no significant differences were observed compared to healthy rats (heart, spleen, lungs, and kidneys), suggesting high biocompatibility of the implanted devices *in vivo*.

According to the micro-CT analysis, the transaxial, coronal, sagittal, and 3D-reconstructed images revealed greater quantities of new bone around multilayer-coated PEEK implants, particularly in the PEEK@QCS/HA/LAP group (Fig. 5A). Further quantitative analysis of the micro-CT data confirmed that the QCS/HA/LAP group had the highest level of BV/TV (bone volume/total volume), Tb.Th (trabecular thickness), and Tb.N (trabecular number), and the lowest level of Tb.Sp (trabecular separation), which are commonly used indexes of new bone formation and bone quality (Fig. 5B). Moreover, undecalcified sections were stained with fluorochromes (ARS and calcein), van Gieson stain, and toluidine blue O (Fig. 5C and D), which showed that new bone formation was particularly elevated in the coated implants groups, especially PEEK@QCS/HA/LAP group, in both 6 and 12 weeks, which was in consistence with micro-CT findings.

For more microscopic analysis, H&E and Masson staining of decalcified sections were performed (Fig. 6A). The results showed numerous granulation tissues around the cavity in the bare PEEK group; while more bone tissue visualized in coating groups and the bone volume ratio is much higher in PEEK@QCS/HA/LAP group. Importantly, Masson staining showed that mature bone matrix (stained in red) was a major component in the PEEK@QCS/HA/LAP group, which indicated that the LAP intercalated coating could promote the mature of new bones. Mechanistically, IF staining was positive for WNT16 and  $\beta$ -catenin in surrounding marrow cells in the PEEK@QCS/HA/LAP group (Fig. 6B), which also exhibited higher collagen-I and OCN levels *in vivo* according to immunohistochemical staining (IHC) staining (Fig. 6C–F).

### 3.6. Antibacterial ability

To examine the antibacterial effects of multilayer-coated PEEK substrates, both gram-positive MRSA and gram-negative *E. coli* were studied. The inhibition zone diameter of PEEK@QCS/HA and PEEK@QCS/HA/LAP groups for MRSA and *E. coli* were about 14 and 22 mm, respectively. By contrast, no bacteriostatic ring was observed in the bare PEEK group (Fig. 7A and B). Meanwhile, the survival rates of MRSA and *E. coli* were significantly lower after co-incubation with coated substrates (Fig. 7A and C). SEM was performed to observe bacterial morphology on the surface of samples. As shown in Fig. 7D, the amounts of MRSA and *E. coli* attached to the coated substrates were reduced. In addition, we evaluated biofilm formation and found obvious red “death” signals, along with decreased green “live” signals, on the QCS contained surface for MRSA and *E. coli*, implying disruption of biofilm integrity by the QCS/HA and QCS/HA/LAP coatings (Fig. 7E).

An *in vivo* implant-based soft tissue infection model was established to evaluate the *in vivo* antibacterial ability of implants. In H&E-stained sections (Fig. 7F), relatively mild inflammation was observed in QCS

contained groups. In the Giemsa-stained sections, residual bacteria in the infected area were dramatically decreased in the PEEK@QCS/HA and PEEK@QCS/HA/LAP groups compared to the PEEK group on day 3 and 7 after the operation, but no significant difference was observed between these two groups (Fig. 7G). Compared to the bare PEEK group, the bacterial survival rates for the planktonic bacteria and bacteria surrounding the infected area in the PEEK@QCS/HA and PEEK@QCS/HA/LAP groups were  $15.51 \pm 1.03\%$  and  $14.39 \pm 0.92\%$ , respectively, on day 3; and  $8.13 \pm 1.08\%$  and  $8.50 \pm 1.11\%$ , respectively, on day 7 (Fig. S12). These results indicated that the two coatings had similarly strong *in vivo* killing effects on MRSA.

### 3.7. Surgical implantation simulation

To test the feasibility of coated PEEK implants for clinical application, the lumbar vertebrae and femur specimens of porcine were utilized to mimic surgical implantation process. The 3D structure of porcine lumbar vertebrae and femur were reconstructed and the well-matched interbody fusion cage and femoral prosthesis were designed (Fig. 8A). After 3D-printing, the obtained implants were coated with QCS/HA/LAP films by LBL process and stained using alcian blue. Then, the implants were inserted with traditional operative approach. After implantation, as is shown in Fig. 8B, the LBL coating onto the implants could be retained in a certain extend. Although the coating on the raised surface might be scratched, the coating on the sunk surface could be retained to further exhibit its functions.

## 4. Discussion

Failure to establish a solid connection between implants and host bone tissues is a serious issue for current implant materials, resulting in implant displacement, cage subsidence, fracture nonunion, and pseudoarthrosis [35,36]. Although PEEK belongs to a new generation of implant materials with excellent biocompatibility and a high elastic modulus (3–4 GPa) comparable to human cortical bones, the bone-to-PEEK interface has weak biological activity and poor osseointegration [2,37]. In the current study, specifically, we focus on one of the most susceptible population, who needs GCs therapy for long-term due to the autoimmune and inflammatory diseases. The precautions against implant failure for those patients are more complicated; both bone ingrowth and infection prevention should be taken into considerations [6,9,38]. To address these issues, we performed RNA-sequencing and identified WNT16 as a novel target in GCs-treated rats. Then, we fabricated a hybrid QCS/HA/LAP coating onto the PEEK surface to improve osseointegration by targeting WNT16. Alongside with the potent antibacterial effects of QCS, a multifunctional therapeutic strategy was established using LBL self-assembly. An organic-inorganic hybrid coating of this nature with molecular targeting ability has rarely been used for implant osseointegration. However, our results could aid the development of advanced orthopedic implants customized by using LBL for multifunctional surface modification.

Mechanistically, the canonical Wnt/ $\beta$ -catenin axis plays a vital role in bone homeostasis. Briefly, secreted Wnt ligands bind to frizzled and Lrp5/6 co-receptors in cell membrane, which promote translocation of stabilized  $\beta$ -catenin into the nucleus, in turn triggering Wnt-targeted gene transcription (e.g., Runx2, Bmp2, and Osx) and thus promoting the osteogenesis of BMSCs and OBs [39–41]. The current study revealed that WNT16 was significantly decreased in GCs-BMSCs (one of the top-3 downregulated genes according to RNA-seq), and its expression was almost 32-fold lower than in Ctrl-BMSCs (Fig. 1C). These results are in line with those of Hildebrandt et al., who demonstrated that GCs decrease the WNT16 level in the OB cell line MC3T3-E1, and that treatment with recombinant WNT16 protein could restore DEX-induced suppression of bone formation in mouse calvaria [42]. Similarly, Ohlsson et al. used WNT16 overexpressed transgenic mice to demonstrate that WNT16 could effectively prevent GCs-induced osteoporosis [43].

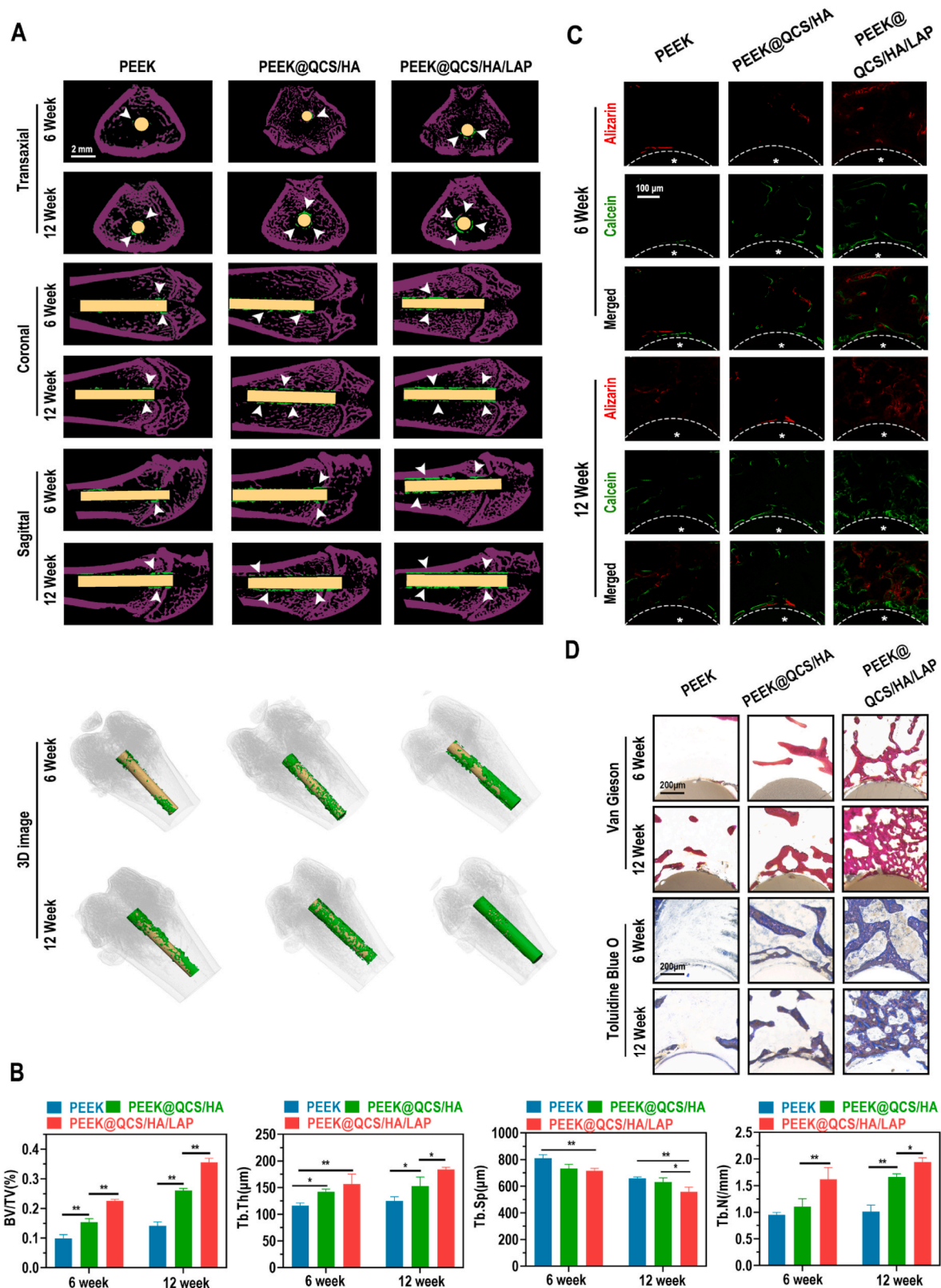


**Fig. 5.** Effects of QCS/HA/LAP coating on new bone formation around the implants (A) Micro-CT results of implants and surrounding bone tissue (transaxial, coronal, and sagittal views, and 3D-reconstructed images). (B) Quantitative analysis of micro-CT data: BV/TV, Tb.Th, Tb.N, and Tb.Sp. (C) Calcein (green) and alizarin red R (red) staining of undecalcified sections. Asterisks indicate the implants and dotted line indicates the implant border, asterisk indicated implants. (D) Van Gieson and toluidine blue O staining of undecalcified sections at 6 and 12 weeks. Data are presented as mean  $\pm$  SD. Significant differences among groups are indicated (\*\* $p < 0.01$ , \* $p < 0.05$ ).

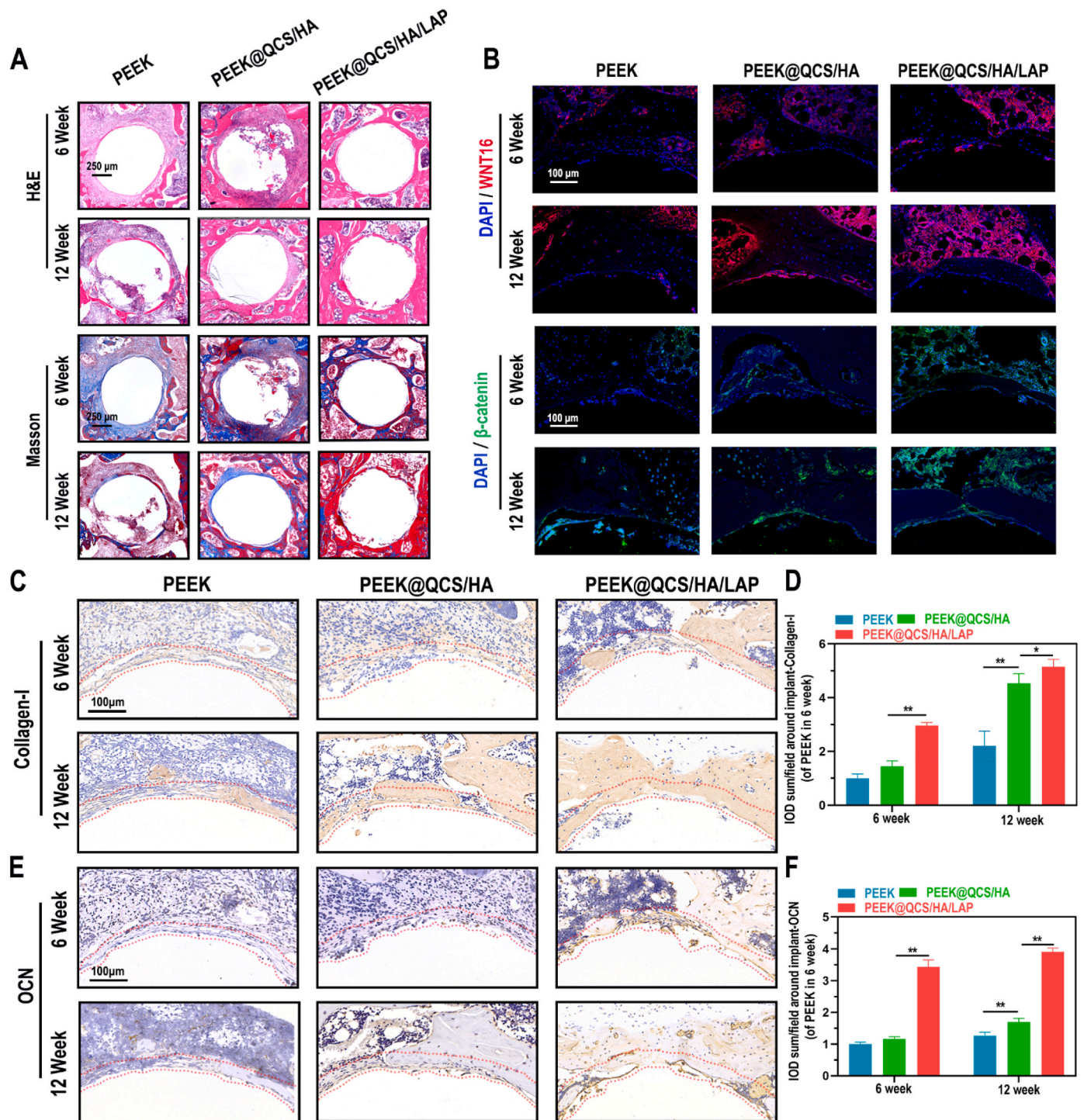


**Fig. 6.** Effects of QCS/HA/LAP coating on WNT16/ $\beta$ -catenin axis *in vivo*. (A) H&E and Masson staining results of peri-implant tissues in various groups at 6 and 12 weeks. (B) IF staining of WNT16 (red),  $\beta$ -catenin (green), and DAPI (blue) of the surrounding bone marrow cells at 6 and 12 weeks. (C–F) IHC-staining and related quantification of Collagen-1 and OCN in regenerative tissue around the implants (red dotted line indicated ROI). Data are presented as mean  $\pm$  SD. Significant differences among groups are indicated (\*\* $p < 0.01$ ).

Instead, the aim of our study was to investigate the role of WNT16 in BMSCs other than OBs using high throughput and *in vitro* experiments, because guided recruitment of endogenous BMSCs and osteogenic differentiation around bone implants are essential for adequate osseointegration [44–46]. Furthermore, among several commercially available 2D nanosheets, MMT, LAP, GO, Mxene and BP were found to promoted WNT16 expression significantly (Fig. 2A). However, based on solution diversity, which is important for continuous LbL, and the high cost of BP

and Mxene, LAP was finally selected as the WNT16 enhancer for composite coating fabrication [30–34]. Due to consisting of  $\text{Li}^+$ ,  $\text{Mg}^{2+}$ ,  $\text{SO}_3^{2-}$ , LAP ( $\text{Na}_{0.7}[(\text{Si}_8\text{Mg}_{5.5}\text{Li}_{0.3})\text{O}_{20}(\text{OH})_4]$ ) was reported possess potent pro-osteogenic capacity, and the underlying mechanism was previously suggested to be associated with canonical Wnt signaling [30,47]. Of note, lithium ion is a classical GSK-3 $\beta$  antagonist that effectively increases  $\beta$ -catenin, but the ion concentration released from LAP is relatively low [28,48]. Interestingly, Mousa et al. recently reported that

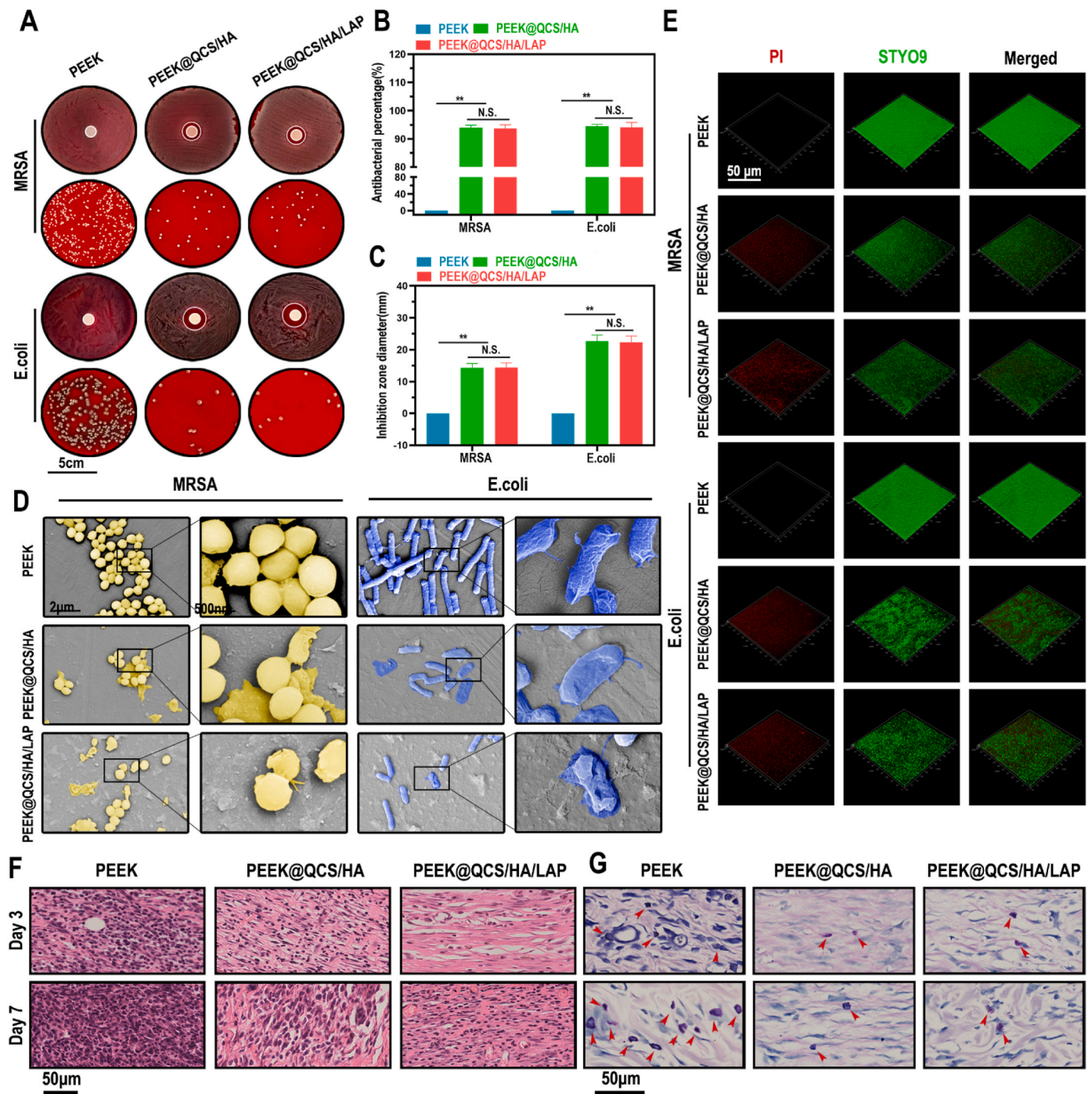


**Fig. 7.** Antibacterial evaluation of PEM coatings (A–C) Antibacterial properties of different surfaces against MRSA and *E. coli* using the agar diffusion test at 12 h (number of bacterial clones and diameter of inhibition zone). (D) SEM images showing the morphology of MRSA and *E. coli* incubated with different PEEK substrates for 24 h. (E) Styo9-PI staining of MRSA and *E. coli* implanted on different PEEK substrates for 24 h. (F–G) H&E and Giemsa staining of peri-implant soft tissues at day 3 and 7 after surgery. Data are mean  $\pm$  SD. Significant differences among groups are indicated (\*\* $p < 0.01$ , \* $p < 0.05$ ).

LAP-mediated osteogenesis is not related to the  $\text{Li}^+$  concentration, which suggests that there may be another underlying mechanism [49]. In line with this, our data revealed that LAP could promote BMSCs osteogenesis in a dose-dependent manner with WNT16 (Fig. 2), which might improve intercellular Wnt signaling transduction (Scheme 1). Although current results could not confirm that the WNT16 mediate all beneficial effects of LAP, this emerging Wnt ligand is of interest for future studies. On the other hand,  $\text{Li}^+$  and  $\text{Mg}^{2+}$  were reported to have anti-apoptotic effects on GCs induced cell death [50,51]. It might be the reason that LAP could reverse GCs inhibited proliferation of BMSCs.

Except for the LAP-mediated enhanced osteogenesis, LbL coating also has several advantages. For example, compared to the highly smooth and relatively inert surface of bare PEEK, both QCS/HA and QCS/HA/LAP coating surfaces exhibited better hydrophilicity and increased roughness. Although it was previously suggested that enhanced surface wettability due to LbL films reduces mammalian and bacterial cell adhesion, this was not applicable to OBs and BMSCs in bone regeneration environments [52]. OB adhesion was increased with a decrease in surface contact angle from  $106^\circ$  to  $0^\circ$  [53], possibly because assembled hydrophilic polyelectrolytes (e.g., CS and HA)

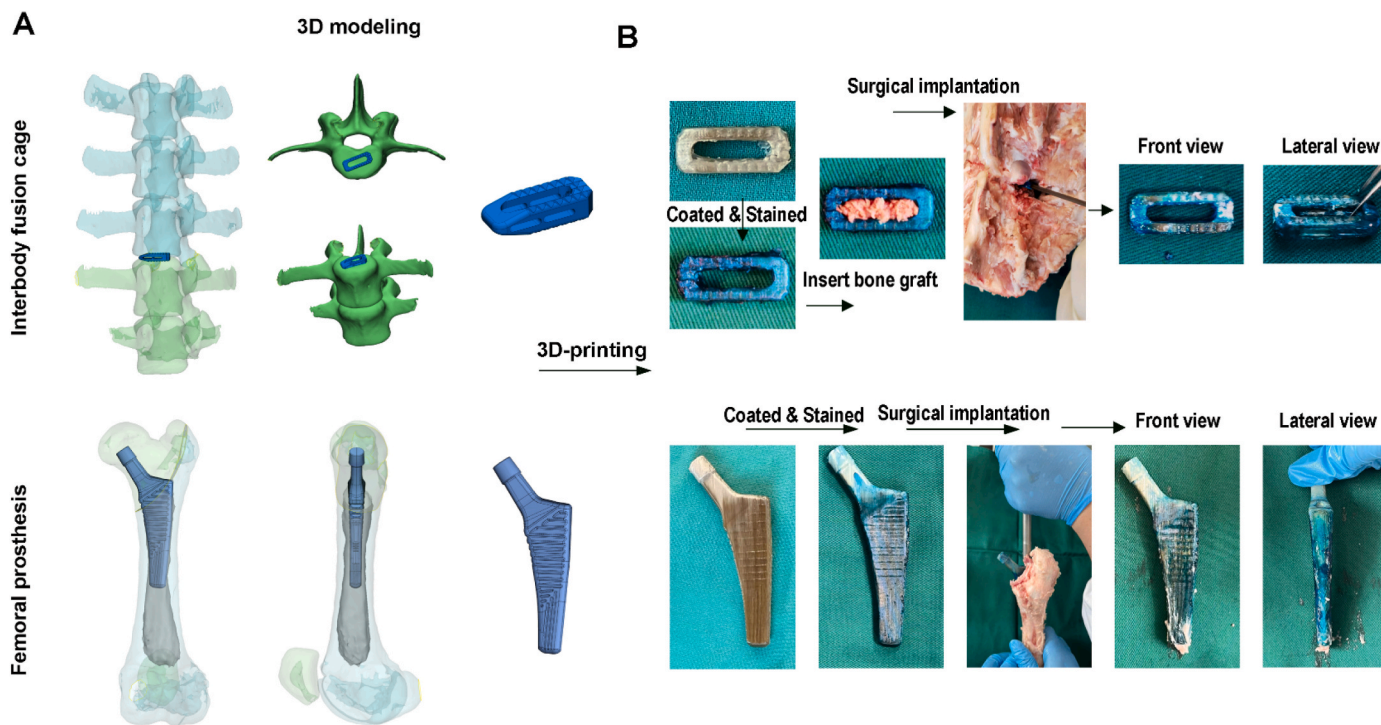


**Fig. 8.** Ex vivo simulation of surgical implantation (A) 3D reconstruction of porcine lumbar vertebrae and femur, and the designed interbody fusion cage and femoral prosthesis. (B) General observation of 3D-printed implants before and after surgical implantation.

promote the absorption of extracellular matrix biomolecules, such as fibronectin and collagen; these molecules determine the degree of initial cell attachment of OBs and BMSCs. On the other hand, numerous studies demonstrated that nanoscale roughness is desirable for mammalian cell adhesion and spreading [54,55]. BMSCs seeded in a nanostructure topography have a more diffuse morphology, which promotes osteogenic differentiation [13,56]. In addition, crosslinking of LbL film is routinely performed to manipulate film characteristics [57]. According to our previous and current studies, slower degradation and enhanced stiffness were observed in LbL films crosslinked by 30 mg/mL of EDC and 11 mg/mL of sNHS mixed solution [58,59]. Several studies have reported that substrate coating with higher stiffness is conducive to the adhesion and osteogenesis of BMSCs, which might be associated with mechanical signaling [57,60]. Moreover, an inorganic nanosheet intercalated structure is superior in terms of surface stiffness compared to pure polymeric structures [20,61]. In accordance with the aforementioned evidence, increased adhesion, a diffuse morphology, and enhanced osteogenesis of BMSCs in coating groups was seen in this study, particularly for the QCS/HA/LAP coated PEEK surface, which had superior hydrophilicity, roughness, and stiffness. These results indicate that LAP intercalated LbL coating is useful to modify the implant surface in a biomimetic microenvironment, to support BMSCs adhesion and differentiation (which enhances osseointegration around the implant).

Peri-implant infection is another disastrous reason leading to implant failure. Especially, infection of implant with a biofilm has been still an unsolved issue in clinical practice [3]. Both gram-positive and -negative bacteria could induce biofilm formation around the implant, and are extremely resistant to antibiotics and host defense mechanisms [3,62]. In the present study, we constructed a multilayer coating with potent antibacterial effects by assembling QCS. As mentioned previously, QCS/HA and QCS/HA/LAP coatings improved the wettability of the implant surface and the later is more hydrophilic than the former, which does not favor bacterial adhesion. However, interestingly, our results show that both coating types could effectively kill *E. coli* and the “super bug” MRSA, and also prevented biofilm formation, both *in vitro* and *in vivo*; but no significant difference was observed between the

groups (Fig. 7). These results indicate that anti-adhesive effects against bacteria due to increased surface hydrophilicity could be neglected in the case of potent QCS, which plays a major role in the defense system.

In addition, it is a common challenge to fabricate an implant coating with highly adhesive strength bonding with substrates, even using the plasma spraying process [63]. In current study, we applied a simple and standard *in vivo* model to test the effects of coating on osseointegration. The intramedullary cavity was firstly created by Kirschner wire, and then the coated PEEK implants were inserted smoothly. Thus, the coatings were not be destroyed during the *in vivo* modeling. To improve the adhesion between coating and substrates, we applied PEI as the precursor layer with a stable positive charge to initial LbL self-assembly process. The adhesive strength of dense PEI coating layer was previously examined by Kim SB et al. using pull-out tests and the results showed reasonably high bonding strength by  $10.8 \pm 1.3$  MPa [64]. Moreover, according to the current micro-scratch test, both QCS/HA and QCS/HA/LAP coating have considerable adhesive strength with PEEK substrates, and the failure load was 2125 mN and 3362 mN, respectively. Meanwhile, QCS/HA/LAP coating displayed higher adhesive strength than QCS/HA coating, indicating that such an inorganic and organic hybrid structure significantly improved the mechanic property.

On the other hand, for the commercial PEEK materials, such as interbody fusion cage and joint prosthesis, their surface were commonly designed with well-aligned topography (wavy or jagged surface) to enhance the frictional force (Fig. 8A). Therefore, though the coating on the raised surface might be scratched, the coating on the sunk surface retained to exhibit its functions. Additionally, in the traditional interbody fusion surgery, the adjacent vertebrae were distracted to create sufficient space for the PEEK cage implantation, which decrease the resistance for cage insertion. Meanwhile, the coating is not only applied for the surface integration, but also coated onto the inner surface of cages, which could directly contact with bone grafts to promote the osteogenesis and finally increased the fusion rate. For the case of femoral joint prosthesis, the marrow cavity was reamed before implants insertion, and not all surface will contact with bone surface during the surgical procedure. Thus, the coating on the distal side of prosthesis were

not be affected by frictional force, but it was also valuable for recruiting intramedullary BMSCs to form a stable bone-to-implant osseointegration. To prove our hypothesis, we supplemented 3D-printing of PEEK cage and femoral joint component based on the porcine lumbar and femur to mimic the surgical implantation. As is shown in Fig. 8B, after implantation, the LBL coating on the implants could be retained in a certain extent according to the alcian blue staining. It indicated that although some coatings would be lost during the implantation process, large part of them could be reserved. In future, however, more stable coating using LBL approach should be proposed to overcome this limitation.

## 5. Conclusion

The purpose of the present study was to fabricate a molecular targeted therapeutic strategy to prevent implant failure in GCs-treated patients. WNT16 is the main contributor to GCs-induced bone loss, and LAP restored its expression in a dose-dependent manner. Accordingly, we introduced LAP into QCS/HA films to fabricate a multifunctional biomimetic coating, which demonstrated increased hydrophilicity and a rough topography. *In vitro*, this hybrid coating not only improved adhesion and osteogenic differentiation of GCs-BMSCs by enhancing WNT16, but also exerted potent bactericidal effects on MRSA and *E. coli*. *In vivo*, the QCS/HA/LAP multilayer coating-modified PEEK implant effectively promoted bone formation around implants in GCs-treated rats. Additionally, after simulating the surgical implantation process *ex vivo*, the coatings onto the 3D printed PEEK implants could be retained in a large part. Taken together, our findings suggest synergistic effects of QCS/HA/LAP coating on osteointegration and peri-implant infections, and shows promise for customized implant design and application.

## Ethics statement

The use of animals in these experiments was in accordance with the Interdisciplinary Principles and Guidelines for the Use of Animals in Research, Testing, and Education. The welfare of the experimental animals was prioritized, and all animal experiments were approved by the Animal Care Committee of Shanghai Jiao Tong University Affiliated Sixth People's Hospital at the Shanghai Jiao Tong University School of Medicine and followed the Animal Research: Reporting of *In Vivo* Experiments (ARRIVE) guidelines.

## Availability of data and materials

The datasets used and/or analyzed during the current study are available from the corresponding author on reasonable request.

## CRediT authorship contribution statement

**Zhe Liu:** Conceptualization, Methodology, Investigation, Formal analysis, Writing – original draft, Visualization. **Qian Tang:** Conceptualization, Methodology, Investigation, Formal analysis, Writing – review & editing, Visualization, Funding acquisition. **Ruo-Tao Liu:** Methodology, Formal analysis, Conceptualization, Software. **Ming-Zhao Yu:** Formal analysis, Software, Validation. **Hao Peng:** Visualization, Software. **Chang-Qing Zhang:** Conceptualization, Supervision, Project administration, Resources. **Zhen-Zhong Zhu:** Methodology, Writing – review & editing, Supervision, Funding acquisition. **Xiao-Juan Wei:** Conceptualization, Writing – review & editing, Data curation.

## Declaration of competing interest

The authors declare that they have no known competing financial interests or personal relationships that could have appeared to influence the work reported in this paper.

## Acknowledgments

This work was supported by Shanghai Sailing Program (22YF1433200) and the National Natural Science Foundation of China (82172400).

## Appendix A. Supplementary data

Supplementary data to this article can be found online at <https://doi.org/10.1016/j.bioactmat.2022.09.013>.

## References

- [1] M. Kumar, R. Kumar, S. Kumar, Coatings on orthopedic implants to overcome present problems and challenges: a focused review, *Materials Today: Proceedings* 45 (2021) 5269–5276.
- [2] H. Ma, A. Suonan, J. Zhou, Q. Yuan, L. Liu, X. Zhao, X. Lou, C. Yang, D. Li, Y.-g. Zhang, PEEK (Polyether-ether-ketone) and its composite materials in orthopedic implantation, *Arabian Journal of Chemistry* 14 (3) (2021).
- [3] M. Chen, H. Sun, H. Ouyang, J.E. Jones, Q. Yu, Y. Xu, S. Revu, Biofilm-inhibiting and Osseointegration-Promoting Orthopedic Implants with Novel Nanocoatings, *Racing for the Surface*, Springer2020, pp. 73–89.
- [4] T. Aghaloo, J. Pi-Anfruns, A. Moshaverinia, D. Sim, T. Grogan, D. Hadaya, The effects of systemic diseases and medications on implant osseointegration: a systematic review, *Int J Oral Maxillofac Implants* 34 (2019) s35–s49.
- [5] Y. He, W. Bao, X.D. Wu, W. Huang, H. Chen, Z. Li, Effects of systemic or local administration of zoledronate on implant osseointegration: a preclinical meta-analysis, *Biomed Res Int* 2019 (2019), 9541485.
- [6] J.H. Fu, J.D. Bashutski, K. Al-Hezaimi, H.L. Wang, Statins, glucocorticoids, and nonsteroidal anti-inflammatory drugs: their influence on implant healing, *Implant Dent* 21 (5) (2012) 362–367.
- [7] P. Chotiaymwong, E.V. McCloskey, Pathogenesis of glucocorticoid-induced osteoporosis and options for treatment, *Nat Rev Endocrinol* 16 (8) (2020) 437–447.
- [8] M.R. Boylan, D.C. Perfetti, R.K. Elmallah, V.E. Krebs, C.B. Paulino, M.A. Mont, Does chronic corticosteroid use increase risks of readmission, thromboembolism, and revision after THA? *Clin Orthop Relat Res* 474 (3) (2016) 744–751.
- [9] K.J. Kebaish, A.R. Galivanche, A.G. Varthi, T.D. Ottesen, L.E. Rubin, J.N. Grauer, Long-term corticosteroid use independently correlates with complications after posterior lumbar spine surgery, *Orthopedics* 44 (3) (2021) 172–179.
- [10] M.M. Bruin, R.L.M. Deijkers, M.P.A. Bus, E.P.M. van Elzakkor, R. Bazuin, R. G. Nelissen, B.G. Pijls, Inhaled corticosteroids, vitamin K antagonists and amlodipine were associated with an increased risk of acute periprosthetic joint infection in patients with total hip arthroplasty: a retrospective case-cohort study, *Journal of Clinical Medicine* 11 (7) (2022).
- [11] D. Alkekha, P.T. Hammond, A. Shukla, Layer-by-Layer biomaterials for drug delivery, *Annual Review of Biomedical Engineering* 22 (1) (2020) 1–24.
- [12] P.T. Hammond, Building biomedical materials layer-by-layer, *Materials Today* 15 (5) (2012) 196–206.
- [13] A.M. Ferreira, C. Tonda-Turo, E. Mancuso, P. Gentile, Multilayer nanoscale functionalization to treat disorders and enhance regeneration of bone tissue, *Nanomedicine* 19 (2019) 22–38.
- [14] X. Zhang, Y. Xu, X. Zhang, H. Wu, J. Shen, R. Chen, Y. Xiong, J. Li, S. Guo, Progress on the layer-by-layer assembly of multilayered polymer composites: strategy, structural control and applications, *Progress in Polymer Science* 89 (2019) 76–107.
- [15] X. Zhu, X. Jun Loh, Layer-by-layer assemblies for antibacterial applications, *Biomater Sci* 3 (12) (2015) 1505–1518.
- [16] P. Gentile, I. Carmagnola, T. Nardo, V. Chiono, Layer-by-layer assembly for biomedical applications in the last decade, *Nanotechnology* 26 (42) (2015), 422001.
- [17] K.-f. Ren, M. Hu, H. Zhang, B.-c. Li, W.-x. Lei, J.-y. Chen, H. Chang, L.-m. Wang, J. Ji, Layer-by-layer assembly as a robust method to construct extracellular matrix mimic surfaces to modulate cell behavior, *Progress in Polymer Science* 92 (2019) 1–34.
- [18] J.J. Richardson, J. Cui, M. Bjornmalm, J.A. Braunger, H. Ejima, F. Caruso, Innovation in layer-by-layer assembly, *Chem Rev* 116 (23) (2016) 14828–14867.
- [19] S. Zhao, F. Caruso, L. Dahne, G. Decher, B.G. De Geest, J. Fan, N. Feliu, Y. Gogotsi, P.T. Hammond, M.C. Hersam, A. Khademhosseini, N. Kotov, S. Loporatti, Y. Li, F. Lisdat, L.M. Liz-Marzan, S. Moya, P. Mulvaney, A.L. Rogach, S. Roy, D. G. Shchukin, A.G. Skirtach, M.M. Stevens, G.B. Sukhorukov, P.S. Weiss, Z. Yue, D. Zhu, W.J. Parak, The future of layer-by-layer assembly: a tribute to ACS nano associate editor helmuth Mohwald, *ACS Nano* 13 (6) (2019) 6151–6169.
- [20] P. Podsiadlo, A.K. Kaushik, E.M. Arruda, A.M. Waas, B.S. Shim, J. Xu, H. Nandivada, B.G. Pumplun, J. Lahann, A. Ramamoorthy, N.A. Kotov, Ultrastrong and stiff layered polymer nanocomposites, *Science* 318 (5847) (2007) 80–83.
- [21] R. Davis, R.A. Urbanowski, A.K. Gaharwar, 2D layered nanomaterials for therapeutics delivery, *Current Opinion in Biomedical Engineering* 20 (2021), 100319.
- [22] A. Murali, G. Lokhande, K.A. Deo, A. Brokesh, A.K. Gaharwar, Emerging 2D nanomaterials for biomedical applications, *Mater Today (Kidlington)* 50 (2021) 276–302.
- [23] Q. Tang, Z. Hu, H. Jin, G. Zheng, X. Yu, G. Wu, H. Liu, Z. Zhu, H. Xu, C. Zhang, L. Shen, Microporous polysaccharide multilayer coated BCP composite scaffolds

- with immobilised calcitriol promote osteoporotic bone regeneration both in vitro and in vivo, *Theranostics* 9 (4) (2019) 1125–1143.
- [24] P. Liu, W. Meng, S. Wang, Y. Sun, M.A. Ashraf, Quaternary ammonium salt of chitosan: preparation and antimicrobial property for paper, *Open Med (Wars)* 10 (1) (2015) 473–478.
- [25] J. Pajarinen, T.H. Lin, A. Nabeshima, E. Jansen, L. Lu, K. Nathan, Z. Yao, S. B. Goodman, Mesenchymal stem cells in the aseptic loosening of total joint replacements, *J Biomed Mater Res A* 105 (4) (2017) 1195–1207.
- [26] W. Chen, G. Xie, Y. Lu, J. Wang, B. Feng, Q. Wang, K. Xu, J. Bao, An improved osseointegration of metal implants by pitavastatin loaded multilayer films with osteogenic and angiogenic properties, *Biomaterials* 280 (2022), 121260.
- [27] K. Turajane, G. Ji, Y. Chinenov, M. Chao, U. Ayturk, V.J. Suhardi, M.B. Greenblatt, L.B. Ivashkiv, M.P. Bostrom, X. Yang, RNA-Seq analysis of peri-implant tissue shows differences in immune, Notch, Wnt, and angiogenesis pathways in aged versus young mice, *JBM R Plus* 5 (11) (2021), e10535.
- [28] Y. Jin, L. Xu, X. Hu, S. Liao, J.L. Pathak, J. Liu, Lithium chloride enhances bone regeneration and implant osseointegration in osteoporotic conditions, *J Bone Miner Metab* 35 (5) (2017) 497–503.
- [29] Y.N. Wang, T.T. Jia, Y. Feng, S.Y. Liu, W.J. Zhang, D.J. Zhang, X. Xu, Hyperlipidemia impairs osseointegration via the ROS/Wnt/beta-Catenin pathway, *J Dent Res* 100 (6) (2021) 658–665.
- [30] S.S. Das, Neelam, K. Hussain, S. Singh, A. Hussain, A. Faruk, M. Tebyetekerwa, Laponite-based nanomaterials for biomedical applications: a review, *Curr Pharm Des* 25 (4) (2019) 424–443.
- [31] G. Kiaee, N. Dimitrakakis, S. Sharifzadeh, H.J. Kim, R.K. Avery, K.M. Moghaddam, R. Haghniaz, E.P. Yalcintas, N.R. Barros, S. Karamikamkar, A. Libanori, A. Khademhosseini, P. Khoshkhalgh, Laponite-based nanomaterials for drug delivery, *Adv Healthc Mater* (2022), e2102054.
- [32] G. Cinelli, G. Bufalo, F. Lopez, L. Ambrosone, Cooperativity between dimerization and binding equilibria in the ternary system laponite-indocyanine green-water, *ChemEngineering* 5 (1) (2021).
- [33] H. Tomás, C.S. Alves, J. Rodrigues, Laponite®, A key nanoplatform for biomedical applications? *Nanomedicine: Nanotechnology, Biology and Medicine* 14 (7) (2018) 2407–2420.
- [34] P. Chen, S. Xu, R. Wu, J. Wang, R. Gu, J. Du, A transparent Laponite polymer nanocomposite hydrogel synthesis via in-situ copolymerization of two ionic monomers, *Applied Clay Science* 72 (2013) 196–200.
- [35] Y.C. Wong, W.W.J. Chau, K.O. Kwok, S.W. Law, Incidence and risk factors for implant failure in spinal metastasis surgery, *Asian Spine J* 14 (6) (2020) 878–885.
- [36] E. Gibon, L. Lu, S.B. Goodman, Aging, inflammation, stem cells, and bone healing, *Stem Cell Res Ther* 7 (1) (2016) 44.
- [37] X. Liu, F. Han, P. Zhao, C. Lin, X. Wen, X. Ye, Layer-by-layer self-assembled multilayers on PEEK implants improve osseointegration in an osteoporosis rabbit model, *Nanomedicine* 13 (4) (2017) 1423–1433.
- [38] A. Premkumar, K. Morse, A.E. Levack, M.P. Bostrom, A.V. Carli, Periprosthetic joint infection in patients with inflammatory joint disease: prevention and diagnosis, *Curr Rheumatol Rep* 20 (11) (2018) 68.
- [39] Y. Chen, B.A. Alman, Wnt pathway, an essential role in bone regeneration, *J Cell Biochem* 106 (3) (2009) 353–362.
- [40] G. Liu, S. Vijayakumar, L. Grumolato, R. Arroyave, H. Qiao, G. Akiri, S. A. Aaronson, Canonical Wnts function as potent regulators of osteogenesis by human mesenchymal stem cells, *J Cell Biol* 185 (1) (2009) 67–75.
- [41] K.S. Houschyar, C. Tapking, M.R. Borrelli, D. Popp, D. Duscher, Z.N. Maan, M. P. Chelliah, J. Li, K. Harati, C. Wallner, S. Rein, D. Pforringer, G. Reumuth, G. Grieb, S. Mouraret, M. Dadrass, J.M. Wagner, J.Y. Cha, F. Siemers, M. Lehnhardt, B. Behr, Wnt pathway in bone repair and regeneration - what do we know so far, *Front Cell Dev Biol* 6 (2018) 170.
- [42] S. Hildebrandt, U. Baschant, S. Thiele, J. Tuckermann, L.C. Hofbauer, M. Rauner, Glucocorticoids suppress Wnt16 expression in osteoblasts in vitro and in vivo, *Sci Rep* 8 (1) (2018) 8711.
- [43] C. Ohlsson, K.H. Nilsson, P. Henning, J. Wu, K.L. Gustafsson, M. Poutanen, U. H. Lerner, S. Moverare-Skrtic, WNT16 overexpression partly protects against glucocorticoid-induced bone loss, *Am J Physiol Endocrinol Metab* 314 (6) (2018) E597–E604.
- [44] H. Xia, X. Li, W. Gao, X. Fu, R.H. Fang, L. Zhang, K. Zhang, Tissue repair and regeneration with endogenous stem cells, *Nature Reviews Materials* 3 (7) (2018) 174–193.
- [45] L. Jiang, W. Zhang, L. Wei, Q. Zhou, G. Yang, N. Qian, Y. Tang, Y. Gao, X. Jiang, Early effects of parathyroid hormone on vascularized bone regeneration and implant osseointegration in aged rats, *Biomaterials* 179 (2018) 15–28.
- [46] Y. Zhang, J. Xu, Y.C. Ruan, M.K. Yu, M. O’Laughlin, H. Wise, D. Chen, L. Tian, D. Shi, J. Wang, S. Chen, J.Q. Feng, D.H. Chow, X. Xie, L. Zheng, L. Huang, S. Huang, K. Leung, N. Lu, L. Zhao, H. Li, D. Zhao, X. Guo, K. Chan, F. Witte, H. C. Chan, Y. Zheng, L. Qin, Implant-derived magnesium induces local neuronal production of CGRP to improve bone-fracture healing in rats, *Nat Med* 22 (10) (2016) 1160–1169.
- [47] X. Zhang, J. Fan, C.S. Lee, S. Kim, C. Chen, M. Lee, Supramolecular hydrogels based on nanoclay and guanidine-rich chitosan: injectable and moldable osteoinductive carriers, *ACS Appl Mater Interfaces* 12 (14) (2020) 16088–16096.
- [48] P.J. Prusick, S.A. Sabri, C.J. Kleck, Expectoration of anterior cervical discectomy and fusion cage: a case report, *J Spine Surg* 7 (2) (2021) 218–224.
- [49] M. Mousa, J.A. Milan, O. Kelly, J. Doyle, N.D. Evans, R.O.C. Oreffo, J.I. Dawson, The role of lithium in the osteogenic bioactivity of clay nanoparticles, *Biomater Sci* 9 (8) (2021) 3150–3161.
- [50] L.Z. Zheng, J.L. Wang, J.K. Xu, X.T. Zhang, B.Y. Liu, L. Huang, R. Zhang, H.Y. Zu, X. He, J. Mi, Q.Q. Pang, X.L. Wang, Y.C. Ruan, D.W. Zhao, L. Qin, Magnesium and vitamin C supplementation attenuates steroid-associated osteonecrosis in a rat model, *Biomaterials* 238 (2020), 119828.
- [51] Y.L. Zhang, Z.Z. Zhu, L.C. Zhang, G. Wang, Lithium chloride prevents glucocorticoid-induced osteonecrosis of femoral heads and strengthens mesenchymal stem cell activity in rats, *Chin Med J (Engl)* 134 (18) (2021) 2214–2222.
- [52] S. Guo, X. Zhu, X.J. Loh, Controlling cell adhesion using layer-by-layer approaches for biomedical applications, *Mater Sci Eng C Mater Biol Appl* 70 (Pt 2) (2017) 1163–1175.
- [53] J. Wei, T. Igarashi, N. Okumori, T. Igarashi, T. Maetani, B. Liu, M. Yoshinari, Influence of surface wettability on competitive protein adsorption and initial attachment of osteoblasts, *Biomed Mater* 4 (4) (2009), 045002.
- [54] R.L. Price, K. Ellison, K.M. Haberstroh, T.J. Webster, Nanometer surface roughness increases select osteoblast adhesion on carbon nanofiber compacts, *J Biomed Mater Res A* 70 (1) (2004) 129–138.
- [55] L. Bacakova, E. Filova, M. Parizek, T. Ruml, V. Svorcik, Modulation of cell adhesion, proliferation and differentiation on materials designed for body implants, *Biotechnol Adv* 29 (6) (2011) 739–767.
- [56] R. McBeath, D.M. Pirone, C.M. Nelson, K. Bhadriraju, C.S. Chen, Cell shape, cytoskeletal tension, and RhoA regulate stem cell lineage commitment, *Dev Cell* 6 (4) (2004) 483–495.
- [57] V.I. Kulikouskaya, S.V. Pinchuk, K.S. Hileuskaya, A.N. Kraskouski, I.B. Vasilevich, K.A. Matievski, V.E. Agabekov, I.D. Volotovskii, Layer-by-layer buildup of polysaccharide-containing films: physico-chemical properties and mesenchymal stem cells adhesion, *J Biomed Mater Res A* 106 (8) (2018) 2093–2104.
- [58] L. Shen, Y. Jiang, Q. Tang, J. Ji, B. Wang, Y. Huang, Z. Qian, Silver nanoparticles reinforced (Poly-(l-lysine)/Hyaluronic acid) free-standing films: the mechanical strength and antibacterial activity, *J Biomed Nanotechnol* 13 (9) (2017) 1069–1081.
- [59] Q. Tang, T. Lim, X.J. Wei, Q.Y. Wang, J.C. Xu, L.Y. Shen, Z.Z. Zhu, C.Q. Zhang, A free-standing multilayer film as a novel delivery carrier of platelet lysates for potential wound-dressing applications, *Biomaterials* 255 (2020), 120138.
- [60] A.S. Mertgen, V.T. Trossmann, A.G. Guex, K. Maniura-Weber, T. Scheibel, M. Rottmar, Multifunctional biomaterials: combining material modification strategies for engineering of cell-contacting surfaces, *ACS Appl Mater Interfaces* 12 (19) (2020) 21342–21367.
- [61] P. Podsiadlo, M. Michel, J. Lee, E. Verploegen, N. Wong Shi Kam, V. Ball, J. Lee, Y. Qi, A.J. Hart, P.T. Hammond, N.A. Kotov, Exponential growth of LBL films with incorporated inorganic sheets, *Nano Lett* 8 (6) (2008) 1762–1770.
- [62] X. Yuan, L. Ouyang, Y. Luo, Z. Sun, C. Yang, J. Wang, X. Liu, X. Zhang, Multifunctional sulfonated polyetheretherketone coating with beta-defensin-14 for yielding durable and broad-spectrum antibacterial activity and osseointegration, *Acta Biomater* 86 (2019) 323–337.
- [63] E. Mohseni, E. Zalnezhad, A.R. Bushroa, Comparative investigation on the adhesion of hydroxyapatite coating on Ti–6Al–4V implant: a review paper, *International Journal of Adhesion and Adhesives* 48 (2014) 238–257.
- [64] S.B. Kim, J.H. Jo, S.M. Lee, H.E. Kim, K.H. Shin, Y.H. Koh, Use of a poly(ether imide) coating to improve corrosion resistance and biocompatibility of magnesium (Mg) implant for orthopedic applications, *J Biomed Mater Res A* 101 (6) (2013) 1708–1715.